# Modeling and Detection of Hotspot in Shaded Photovoltaic Cells

**Rossi, D., Omana, M., Giaffreda, D. and Metra, C.**

This is a copy of the author's accepted version of a paper subsequently published in *IEEE Transactions on Very Large Scale Integration (VLSI) Systems,* 23 (6), pp. 1031-1039.

It is available online at:

https://dx.doi.org/10.1109/TVLSI.2014.2333064

# Modeling and Detection of Hot-Spot in Shaded Photovoltaic Cells

D. Rossi, M. Omaña, D. Giaffreda, and C. Metra

***Abstract*— We address the problem of modeling the thermal behavior of photovoltaic (PV) cells undergoing a hot-spot condition. In case of shading, in fact, PV cells, may experience a dramatic temperature increase, with consequent reduction of the provided power. Our model has been validated against experimental data, and has highlighted a counterintuitive PV cell behavior, that should be taken into account to improve the energy efficiency of PV arrays. Then, we propose a hot-spot detection scheme, enabling to identify the PV module that is under hot-spot condition. Such a scheme can be used to avoid the permanent damage of the cells under hot-spot, thus their drawback on the power efficiency of the entire PV system.**

***Index Terms*— Energy efficiency, hot-spot, PV systems, reliability.**

## I. Introduction

In recent years, photovoltaic (PV) arrays have been increasingly adopted in the urban environment, as a promising source of green energy. In such an environment, (partial) shading of the PV array from nearby obstructions, such as trees, telephone poles, antennas, neighboring buildings, or from bird droppings, tree leaves, etc., is very frequent. The shading of a PV cell, or of a group of cells can lead to a phenomenon denoted as hot-spot. This can produce a permanent damage of the shaded cell, with a consequent reduction of the provided power [1, 2].

Hot-spot takes place when one, or more PV cells within a PV module are shaded, with a consequent mismatch in the irradiation of the cells in the module. Under this condition, the non-shaded part of the module operates at current levels higher than those of the shaded PV cells. As a consequence, the affected cells are forced into reverse bias and starts to dissipate power, with a consequent temperature increase. This causes the overheating (hot-spot) of the PV cells. If the shading condition is not removed before that the cell temperature reaches a critical value, the shaded PV cells can be permanently damaged [3]. In some cases, the reverse bias voltage can reach the breakdown voltage of the cell, thus leading to its destruction in a few tens of seconds [3]. As a result, an open circuit appears at the serial branch to which the cell is connected [4]. If the PV module containing the damaged cell(s) is connected in series to other PV modules, the open circuit due to the hot-spot will eventually disconnect the whole branch containing the affected PV module from the PV system [4]. This will cause a considerable decrease in the energy provided by the whole PV system.

To counteract the detrimental effect of shading, bypass diodes are usually connected in antiparallel with the PV cells [2, 5] in an array. These bypass diodes limit the reverse voltage that can be applied to a PV cell, thus preventing it from reaching the breakdown voltage when shaded. However, it has been proven that hot-spot conditions may still occur, even if bypass diodes are adopted [3]. In fact, due to defects and impurities within the silicon, some PV cells may exhibit a large reverse current, even before reaching the breakdown voltage. This phenomenon is usually modeled by inserting a parallel shunt resistance, whose value depends on the concentration and distribution of defects/impurities within the PV cell. If the shunt resistance is low enough, a hot-spot condition can occur even before that the PV cell enters the breakdown region [2, 3, 6]. In this case, due to the hot-spot heating, the PV cell can reach a temperature high enough to cause its permanent damage [2, 3, 6], although this takes longer to occur than when the PV cell operates in breakdown.

The time required by the heating to generate a permanent damage in a PV cell under hot-spot depends strongly on environmental parameters and impurities in the materials [7]. Such a time should be known to activate possible countermeasures to avoid the PV cell permanent damage, thus the consequent loss of efficiency of the whole PV array.

So far, a few approaches have been proposed to detect the hot-spot condition [8, 9]. In [8, 9], a novel PV module structure, and a hot-spot detection scheme are proposed. Detection is based on current monitoring, followed by a comparison with a computed theoretical value, enabling to identify the cells under hot-spot. The correct computation of the current theoretical value is however a critical issue, given its strong dependence on environmental parameters.

Based on these considerations, in this paper we propose a new approach to detect the occurrence of hot-spot to allow the application of possible countermeasures to avoid the permanent damage of the cells under hot-spot. To achieve this goal, first we describe a model that we have preliminary introduced in [10],to estimate the temperature of a PV cell, as a function of the time interval in which it is under hot-spot.

Manuscript submitted March 21, 2014.
D. Rossi, M. Omaña, D. Giaffreda and C. Metra are with the Department of Electrical, Electronic and Information Engineering, University of Bologna, 40136, Bologna, Italy (e-mail: d.rossi@unibo.it; martin.omana@unibo.it; daniele.giaffreda2@unibo.it; cecilia.metra@unibo.it).

Our model has been validated against experimental results. It shows that the time required to reach a critical temperature in the cell area under hot-spot is strongly influenced by shadowing grade, irradiation intensity, ambient temperature, and concentration of impurities in the materials.

Then, we propose a novel scheme to detect the hot-spot condition affecting a cell (or multiple cells). The proposed scheme is conceived as connected to the Maximum Power Point Tracker (MPPT) of each PV module, for PV systems adopting distributed MPPT to allow the maximization of the PV system efficiency [11]. Our detection scheme enables also the quick and unambiguous identification of the PV module containing the cell(s) undergoing a hot-spot condition. The output signals generated by our detection scheme can be used to activate proper countermeasures. As an example, the affected module could be properly bypassed, thus avoiding the permanent damage of the cells under hot-spot and its consequent impact on the efficiency of the whole PV array. The development of such countermeasures is however out of the target of this paper.

The rest of the paper is organized as follows. In Section II, we introduce some basics on PV cells and hot-spot heating. In Section III, we present our model to estimate the temperature of a PV cell as a function of the time interval during which it is under a hot-spot condition, and we validate it against experimental data. In Section IV, by applying our model, we show the thermal behavior of shaded PV cells undergoing hot-spot conditions, and we compare partial shading to full shading effects. In Section V, we describe our proposed hot-spot detection scheme, and report show some results of the simulations that we have performed to verify its behavior. Finally, in Sect. VI we give some conclusive remarks.

## II. PV Cell Hot-Spot Heating

### A. PV Cell Electrical Model

We consider the PV cell standard double diode electrical model in [2, 12], as shown in Fig. 1(a). When the PV cell is exposed to sunlight, it generates a photocurrent given by [13, 14, 15]:

$$I_{ph}=(J_{ph}\cdot A_{cell}\cdot G_{irr})/G_{max}\,, \quad (1)$$

where $G_{irr}$ [W/m$^2$] is the solar irradiation, $J_{ph}$=3.43 [μA/m$^2$] is the maximum photocurrent density for the maximum solar radiation $G_{max}$=1000W/m$^2$, and $A_{cell}$ [m$^2$] is the area of the PV cell. Diodes D1 and D2 account for the saturation mechanisms in the PV cell [1, 8]. Particularly, $I_{D1}$ is the saturation current due to the diffusion mechanism, while $I_{D2}$ is the saturation current generated by the recombination in the space charge layer. The current $I_{RSH}$ represents the leakage current of the PV cell, which is accounted for by the shunt resistance $R_{SH}$ [2, 13]. The resistance $R_S$ models the voltage drop across the PV cell produced by the current $I_{PV}$ [8]. Therefore, the current $I_{PV}$ provided by the PV cell to its load is given by:

$$I_{PV} = I_{ph} - I_{D1} - I_{D2} - I_{RSH}. \quad (2)$$

When a PV cell is biased in the reverse breakdown region, its behavior is modeled by the current generator $I_{BD}$, whose produced current is controlled by the output voltage $V_{PV}$. More in details, $I_{BD}$ is approximately equal to 0A for values of $V_{PV}$ higher than the cell breakdown voltage ($V_{BD}$). Instead, for values of $V_{PV}$ lower than $V_{BD}$ [2], it is:

$$I_{BD} \cong \alpha\cdot(V_{PV}/R_{SH})\cdot(1-(V_{PV}/V_{BD}))^{-m}.$$

Parameters $\alpha$ and $m$ are fitting parameters having the following values: $\alpha$=1.93, $m$ =1.10 [2].

Fig. 1(b) shows the current $I_{PV}$ as a function of $V_{PV}$, for a PV cell modeled by the circuit in Fig. 1(a). The curves have been derived considering a solar irradiation $G_{irr}$=500W/m$^2$, generating a photocurrent $I_{ph}$ =4A, and three different values of the shunt resistance $R_{SH}$. When $V_{pv}$ = 0V, it is $I_{PV}$ = $I_{ph}$ = 4A. In this case, in fact, no current flows through $R_{SH}$ ($I_{RSH}$ =0), and D1 and D2 are off ($I_{D1}$=$I_{D2}$=0). Additionally, also when 0 < $V_{PV}$ < 0.6V, it is $I_{PV} \approx I_{ph}$, since D1 and D2 are still off and $I_{RSH}$ is very small. Instead, for $V_{PV}$ > 0.6V, the current $I_{PV}$ start to decrease quickly as $V_{PV}$ increases, since D1 and D2 become conductive, and $I_{D1}$ and $I_{D2}$ increase quickly as $V_{PV}$ increases. From Fig. 1(b) we can also observe that, when the PV cell is reverse biased ($V_{PV}$ <0), the current $I_{PV}$ increases with the decrease of $V_{PV}$. Moreover, it can be noticed that the value of $I_{PV}$ strongly depends on the value of the shunt resistance $R_{SH}$. In particular, $I_{PV}$ increases faster, when the value of $R_{SH}$ diminishes.

It is worth noticing that, when the PV cell is reverse biased, the absolute value of $V_{PV}$ can be as high as 10 V, so that the power dissipated by the PV cell can be very high [2], and the temperature of the PV cell can considerably increase.

When the PV cell is reverse biased, $I_{PV}$ is non-homogeneously distributed throughout the cell area, and concentrates in small regions (with an area approximately equal to 100μm$^2$) of slightly higher conductivity, where the silicon presents a higher concentration of defects/impurities

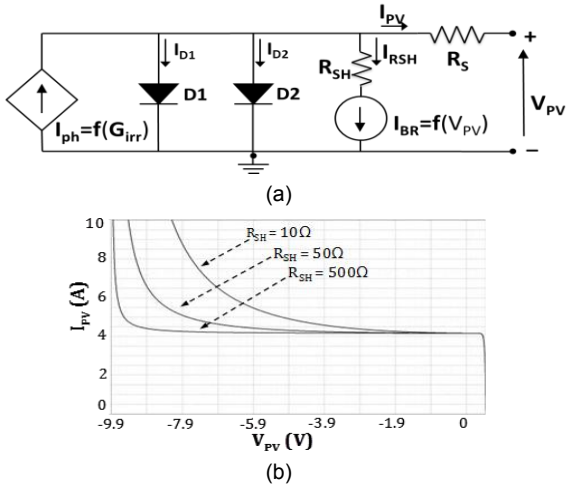


Fig. 1. (a) Considered electrical model for PV cells. (b) $I_{pv}$ as a function of $V_{pv}$ for three different values of $R_{sh}$, with $G_{irr}$=500W/m$^2$ and $I_{ph}$=4A.

[3, 7, 16].

This physical phenomenon is taken into account in the value of the shunt resistance $R_{SH}$. A low value of $R_{SH}$ will originate a large value of $I_{PV}$ when the cell is reverse biased, which will produce a high power dissipation on $R_{SH}$. Such a power dissipation can produce a considerable increase in the temperature of the regions of the PV cell that are close to the impurity centers, thus giving rise to hot-spot heating [6, 12]. Under hot-spot, the temperature of the heated regions can exceed the maximum value tolerated by the PV cell, and can be permanently damaged [2, 3, 6].

To enter a hot-spot condition, a PV cell must be reverse biased. This is likely to occur in typical PV arrays, where many PV cells are connected in series to obtain an adequate level of DC voltage [9, 17].

### B. PV Module Architecture and MPPT Scheme

Several PV module and array architectures have been proposed in the literature [11, 18, 19]. We here consider the approach based on distributed MPPT since, as highlighted in [11], it allows to maximize the PV system efficiency.

#### 1) PV Module architecture with Distributed MPPT

We consider the PV array scheme as reported in Fig. 2 [11]. It is composed by a series of 36 identical PV cells ($PV_i$, i=1..36), with 2 bypass diodes ($DBYP_i$, i=1, 2), each connected in parallel to 18 PV cells [2]. The bypass diodes avoid that a shaded PV cell, which is reverse biased, can enter its breakdown region. In fact, the reverse voltage of a shaded PV cell within the array in Fig. 2, which is equal to the sum of the forward voltages of the other 17 non shaded PV cells sharing the same bypass diode, is always lower than its breakdown voltage $V_{BR}$ (typically equal to -10V).

#### 2) The MPPT

The MPPT absorbs the DC power from the PV array and transfers it to the battery. The main function of the MPPT is to adjust the current and voltage of the PV module, denoted by $I_{mod}$ and $V_{mod}$, respectively (Fig. 2), in order to maximize the power produced by the PV array for any given solar irradiation $G_{irr}$.

The MPPT is usually implemented by means of a DC-DC converter [5, 13, 14], such as the step down DC-DC buck converter shown in Fig. 3, which allows to convey the power produced by the PV module to the battery. It is composed by a transistor M1 acting as a switch, and a freewheeling diode D. As for the components $L$ and $C_{in}$, they filter out spikes on the current provided to the battery, and oscillations on the voltage $V_{mod}$ produced by the PV module, respectively, both induced by the switching of M1 and D.

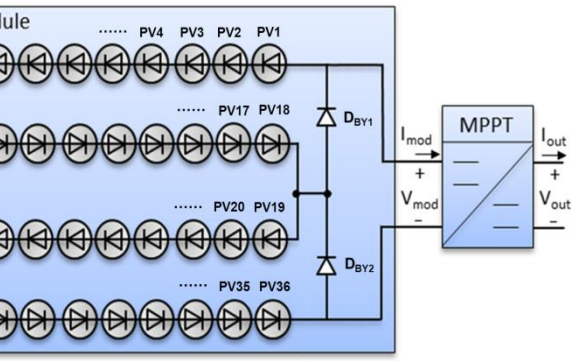


Fig. 2. Considered PV module architecture with distributed MPPT.

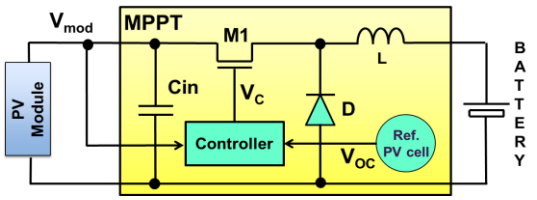


Fig. 3. Schematic representation of the considered step-down buck converter implementing the MPPT circuit.

The *Controller* generates a periodic control signal ($V_C$) with variable duty-cycle allowing to modulate the time during which M1 is on, during each period of $V_C$. This enables to control the average current absorbed from the PV module, as well as the voltage $V_{mod}$, thus making the PV module work at its Maximum Power Point (MPP). In our example, the Controller implements the open-voltage tracking method [15, 17] that, for its simple implementation and low cost, is often employed in PV systems [15]. This method exploits the linear relationship existing between the voltage at which a cell maximizes the generated power ($V_{MPP}$) and its open circuit voltage ($V_{OC}$). In particular, it is always $V_{MPP} = 0.76V_{OC}$, for any solar irradiation $G_{irr}$. Therefore, in order to make the cells of the PV module work at their MPP, the *Controller* compares the voltage of the cells of the array ($V_{cell}$) with the $V_{OC}$ of a reference cell operating under the same $G_{irr}$ as the PV module. Based on the comparison result, the controller adjusts the duty-cycle of $V_C$ so that $V_{cell} = 0.76$ and $V_{OC} = V_{MPP}$ [16]. Finally, in order to obtain $V_{cell}$, the controller simply divides the voltage $V_{mod}$ by the number of cells connected in series in the module.

## III. Model Description and Validation

As described in the previous section, when one PV cell within a series of PV cells is shaded, the power generated by the reverse current of the cell is therefore dissipated in a small area close to impurity centers [7]. Fig. 4(a) shows a representation of the shaded PV cell. The area of the whole PV cell is denoted by $A_{cell}$, while the area of the regions involved by hot-spot heating is denoted by $A_{HS}$. In particular, $A_{HS}$ represents the area of the region of the PV cell around the impurity centers experiencing a considerable temperature increase when the PV cell is partially/fully shaded. The value of $A_{HS}$ depends on the PV cell fabrication process, and has been experimentally proven to be usually in the range of 5%-10% of $A_{cell}$ [20].

Our model, as preliminarily described in [10], consists of two series thermal RC circuits. The lower *RC* circuit (composed by $C_{THcell}$ and $R_{THcell}$) accounts for the temporal behavior of the PV cell temperature as a function of solar irradiation ($T_{cell}$ in Fig. 4(b)) only. Instead, the upper thermal

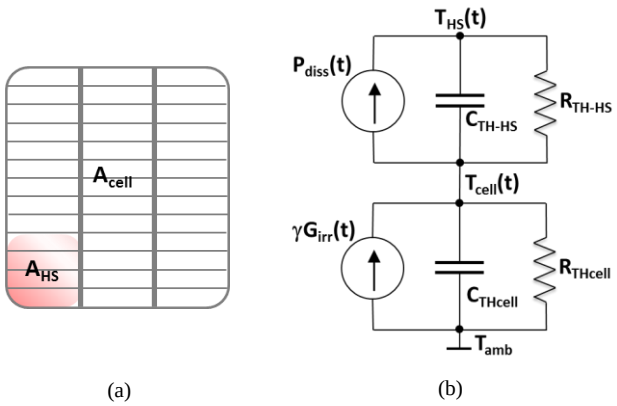


(a) (b)

Fig. 4 (a) Partial shaded PV cell undergoing hot-spot condition; (b) Equivalent thermal model to estimate the time dependence of the temperature of the portion of the PV cell ($A_{HS}$) under hot-spot condition.

*RC* circuit (composed by $C_{TH\text{-}HS}$ and $R_{TH\text{-}HS}$) models the temporal behavior of the area $A_{HS}$ of the PV cell under hot-spot condition, as a function of the power dissipated ($P_{diss}$) on the shunt resistor $R_{SH}$. Particularly, $P_{diss}$ is estimated by SPICE simulations as the power dissipated on the shunt resistance, that is: $P_{diss} = R_{SH} \cdot I_{SH}^2$ [W/m$^2$], where $I_{SH}$ is the reverse bias current of the shaded PV cell.

As for the other parameters in Fig. 4(b), $T_{HS}$ [˚C], $R_{TH\text{-}HS}$ [˚C·m$^2$/W] and $C_{TH\text{-}HS}$ [˚C· m$^2$·sec/W] are the temperature, thermal resistance and thermal capacitance, respectively, of the PV cell portion $A_{HS}$; $T_{cell}$ [˚C], $R_{THcell}$ [˚C·m$^2$/W] and $C_{THcell}$ [˚C·m$^2$·sec/W] are the temperature, thermal resistance and thermal capacitance, respectively, of the remaining portion (not undergoing a hot-spot condition) of the shaded PV cell; $T_{amb}$ [˚C] is the ambient temperature; $G_{irr}$ [W/m$^2$] is the solar radiation density illuminating the PV cell.

The values of parameters $R_{TH\text{-}HS}$, $R_{THcell}$, $C_{TH\text{-}HS}$ and $C_{THcell}$ depend on the materials composing the upper layers of the PV cell (i.e., mainly EVA, glass, etc.). Since most of the heat produced by the PV cell is dissipated on the glass layer [21], we can reasonably assume that the values of these parameters depend only on the properties of the glass layer covering the cell. Therefore, they can be calculated as follows [21]:

$$R_{THcell} = \frac{l}{k \cdot A_{cell}} \qquad R_{TH-HS} = \frac{l}{k \cdot A_{HS}}$$
$$C_{THcell} = A_{cell} \cdot l \cdot \rho \cdot \varsigma \qquad C_{TH-HS} = A_{HS} \cdot l \cdot \rho \cdot \varsigma \tag{3}$$

where $l$ [m] is the thickness of the glass covering the PV cell; $k$ is the glass thermal conductivity; ρ [Kg/m$^3$] is the glass density; ς [J/Kg·˚C] is the glass specific heat capacity.

From the thermal circuit in Fig. 4(b), we can derive the behavior over time of the temperature $T_{HS}$ in the area of the PV cell that is shaded, thus undergoing a hot-sport condition, at a generic time instant denoted by $t_{HS}$, as follows:

$$T_{HS}(t) = \begin{cases} T_{amb} + R_{THcell} G_{irr} & t < t_{HS} \\ T_{amb} + R_{THcell} G_{irr} \left( \gamma + (1-\gamma) e^{-\left(\frac{t-t_{HS}}{R_{THcell} C_{THcell}}\right)} \right) + & \\ + P_{diss} R_{TH-HS} \left( 1 - e^{-\left(\frac{t-t_{HS}}{R_{TH-HS} C_{TH-HS}}\right)} \right) & t \geq t_{HS} \end{cases} \tag{4}$$

where $\gamma = G_{irr\text{-}shaded}/G_{irr}$ denotes the relative mismatch in the irradiation between the shaded ($G_{irr\text{-}shaded}$) and non-shaded ($G_{irr}$) cells of the PV array. Thus, a fully shaded PV cell will present $\gamma = 0$, while for non-shaded PV cells it is $\gamma = 1$.

It is worth noting that the time $t_{HS}$ represents the (arbitrary) generic instant when a hot-spot condition occurs. For $t < t_{HS}$ (that is before the PV cell is shaded and enters a hot-spot condition), the cell works with the same solar irradiation $G_{irr}$ as the other PV cells in the panel, with $\gamma = 1$, so that it is forward biased. In this case, it is $P_{diss} \approx 0$, and $A_{HS} = 0$, and the equivalent circuit coincides with the lower RC circuit in Fig. 4(b). Therefore, the cell temperature turns out to depend only on the solar irradiation. It is:

$$T_{HS} = T_{cell} = T_{amb} + R_{THcell} \cdot G_{irr}.$$

On the other hand, we can observe that after the PV cell is shaded and enters a hot-spot condition (for $t \geq t_{HS}$), there are two different phenomena determining the temperature of the PV cell: i) the contribution of the reduced solar irradiation (i.e., the second term in (4) for $t \geq t_{HS}$), which tends to reduce the PV cell temperature with a time constant $\tau_{cell} = R_{THcell} \cdot C_{THcell} = l \cdot \rho \cdot \varsigma / k$ [sec]; ii) the contribution of the power dissipated by $R_{SH}$ ($P_{diss}$) (i.e., the third term in (4) for $t \geq t_{HS}$), which tends to increase the PV cell temperature with a time constant $\tau_{HS} = R_{TH\text{-}HS} \cdot C_{TH\text{-}HS} = l \cdot \rho \cdot \varsigma / k$ [sec]. As shown in [10], the contribution of ii) to the temperature $T_{HS}$ is considerably higher than the contribution of i). As a result, when a PV cell is shaded, its temperature $T_{HS}$ tends to increase very quickly

Our thermal model (Fig. 4(b)) can be simulated by means of electrical simulation tools, such as SPICE. To this aim, the units of the obtained voltages (currents) must be converted to temperature (power) units, so that 1V (1A) in the simulated electrical circuit corresponds to 1˚C (1W) in the thermal circuit. To summarize, our model allows to evaluate simply and quickly the maximum time interval in which a PV cell can remain under a hot-spot condition, without suffering from permanent damages due to excessive temperature.

We have compared the results obtained using our model to the experimental data reported in [22, 23], considering the same operating conditions and the cell parameters in [22]. Fig. 5 shows the temperature behavior of a shaded cell obtained by our model. We can observe that, before the cell is shaded at time $t_1$, it presents a constant operating temperature of 60˚C, with an ambient temperature of 25°C. This is in very good agreement with the operating temperature of a non-shaded PV cell reported in [22], which reaches T=57.2°C with an ambient temperature of 20°C. After the cell is shaded (at time $t_1$), our model estimates a time interval $\Delta t = t_1 - t_2 = 21.1$s for the operating temperature of the area of the cell under hot-spot to

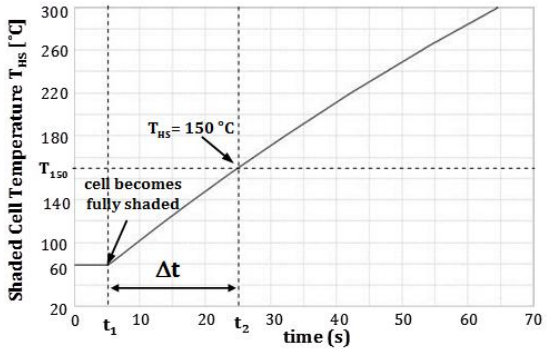


Fig. 5. Temperature trend over time in the fully shaded cell, for the operating conditions reported in [23].

rise by 90˚C, thus reaching a temperature of 150˚C. This result is also in accordance with the experimental data in [23], which reports a thermal behavior of e cell under hot-spot exhibiting a temperature increase of 90°C in approximately 18s. The small difference is due to the different PV cell parameters. Therefore, the proposed model allows to predict the time required by a PV cell to enter a hot-spot condition rather accurately.

We further validated the proposed model with the results reported in [24]. We considered the same power dissipation of 15.1W in the hot-spot area of the shaded PV cell. The obtained results are depicted in Fig. 6. As can be seen, after 1000s, a temperature variation equal to ΔT = (237 – 60)°C= 177°C is achieved, while in [24] a ΔT = 183°C is reported. Therefore, the proposed model enables an accurate evaluation of the thermal transient of a PV cell undergoing a hot-spot condition.

## IV. Thermal Behavior Derived from Our Model

In this section, we have considered the same PV module reported in Fig. 2. As an example, for our analysis we have assumed that the cell PV36 is either almost fully shaded ($\gamma$ =0.01), or partially shaded ($\gamma$ =0.3). Of course similar results would have been obtained considering another PV cell in the module.

We have modeled the PV cells of the module with the electrical circuit shown in Fig. 1(a), considering the following values for its parameters [5]: $V_{BD}$ = -10V; α=1.93; m =1.10,

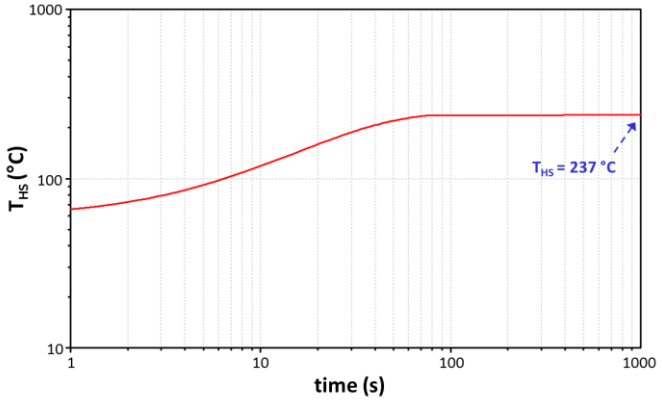


Fig. 6. Temperature trend over time in the fully shaded cell, for the operating conditions reported in [24].

$R_{SH}$ =139.6Ω, $R_S$ = 10mΩ. Additionally, for each one of the 18 PV cells, we have considered a typical area of $A_{cell}$ = 243cm$^2$, from which we can derive a typical $A_{HS}$ = 14cm$^2$, equal to the 6% of $A_{cell}$ [20].

Then, from the equations in (3), the following parameter values are obtained: $R_{THcell}$ = 1.4°C/W; $R_{TH\text{-}HS}$ = 14°C/W; $C_{THcell}$ = 65.5 Ws/°C; $C_{TH\text{-}HS}$ = 6.5 Ws/°C. As first step, by means of electrical level simulations performed by SPICE, we have estimated the power dissipation on the shunt resistance $R_{SH}$ of the shaded PV cell (i.e., PV36) for the two considered cases: 1) when PV36 is almost fully shaded ($\gamma$ =*0.01*); 2) when PV36 is partially shaded ($\gamma$ =*0.3*). The obtained values of dissipated power have then been employed in our thermal model (Fig. 4(b) and (6)) to evaluate the temperature $T_{HS}$ of the shaded cell PV36, as a function of time. In particular, we have used our model to evaluate the time required by the temperature $T_{HS}$ of PV36 to reach *150°C* (hereafter denoted by $T_{150}$) from the beginning of its partial/full shading, where $T_{150}$ is the minimal value of temperature that can cause permanent damage to the PV cell, in case of hot-spot heating [6].

Fig. 7(a) shows the results obtained in case of full shading (γ=0.01) of PV36, and for different values of its shunt resistance $R_{SH}$. Particularly, we considered five possible values of $R_{SH}$, with a ±20% variation with respect to its nominal value. In fact, as stated in Sect. II, the shunt resistance may considerably vary for different impurity concentrations and distributions within a PV cell [7, 16]. The initial irradiation is uniform for the whole module at the maximum value $G_{irr}$=1000W/m$^2$, and the produced temperature is $T_{HS}$=60˚C on all cells. At instant $t_{1FS}$ = 5s the cell PV36 is completely shaded ($G_{irr}$=10W/m$^2$), while the other cells keep on being fully irradiated (thus obtaining γ=0.01). As can be seen, the time interval $\Delta t_{FS}$ required by $T_{HS}$ to reach the critical temperature $T_{150}$ (at time $t_{2FS}$) strongly depends on the value of $R_{SH}$. In the worst case (represented by the lowest value of $R_{SH}$ = 112Ω), it is: $\Delta t_{FS}$ = $t_{2FS}$ − $t_{1FS}$ = 40s. For larger values of $R_{SH}$, $\Delta t_{FS}$ decreases, being approximately $\Delta t_{FS}$ = 65s for the highest value of $R_{SH}$ = 167Ω.

Similarly, Fig. 7(b) depicts the trend over time of the $T_{HS}$ of PV36 when, starting from the time instant $t_{1PS}$ = 5s, it is partially shaded (with $G_{irr}$=300W/m$^2$, thus $\gamma$=0.3), for $R_{SH}$ = 112Ω (i.e., $R_{SH}$ fixed at the lowest value considered in Fig. 7(a)). It is worth noticing that the temperature of the partially shaded cell PV36 increases faster than that of the fully shaded cell shown in Fig. 7(a). Particularly, it is $T_{HS}$ = $T_{150}$ after a time interval equal to $\Delta t_{PS}$= $t_{2PS}$ − $t_{1PS}$ =36s < $\Delta t_{FS}$. This counterintuitive behavior highlighted by our model can be explained from a physical point of view by considering that, in the partially shaded cell, the full irradiation of part of the cell shortens the time needed to enter the hot-spot condition.

## V. Proposed Hot-Spot Detection Scheme

In this section we propose a scheme to detect a hot-spot condition affecting a cell (or multiple cells) within a PV module. Our scheme is based on the observation that, when a hot-spot condition occurs (due to full or partial shading), the

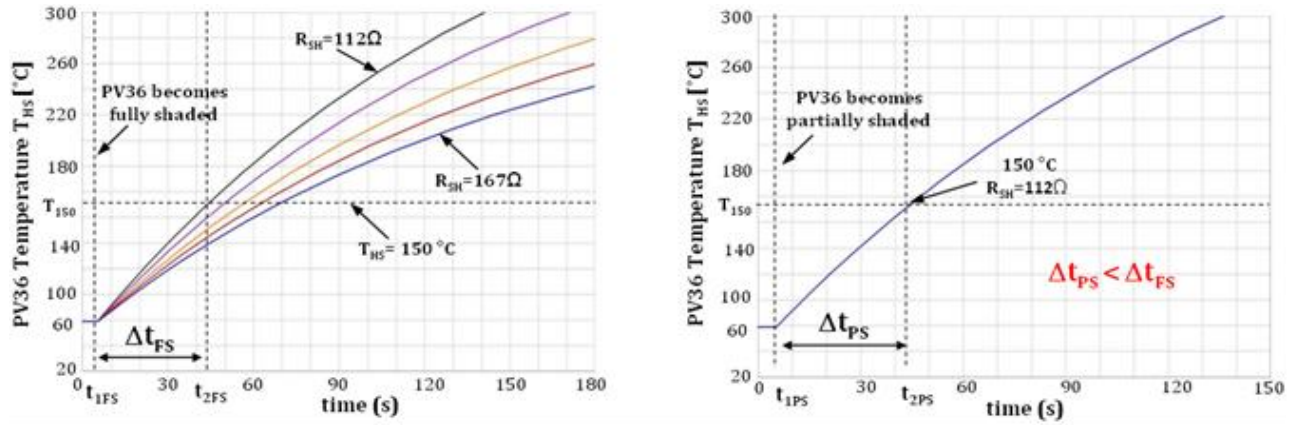


(a) (b)

Fig. 7. Results obtained with our model for the behavior of the $T_{HS}$ temperature of PV36 when: (a) PV36 becomes fully shaded after $t_{1FS}$ = 5s (γ=0.01) and for various values of $R_{SH}$; b) PV36 becomes partially shaded after $t_{1PS}$ = 5s (with γ=0.3) and with the lowest value of $R_{SH}$ =112Ω (worst case condition for the cell temperature).

current provided by the PV module, $I_{mod}$, varies considerably depending on the shading condition.

On the other hand, the voltage $V_{mod}$ is maintained at a constant value by the MPPT. In fact, the controller block of the MPPT regulates the control signal $V_C$ (Fig. 3) in order to maintain the voltage $V_{mod}$ equal to 0.76 $V_{OC}$, where $V_{OC}$ is the open circuit voltage of a reference cell.

In this regard, let us consider the case of a cell of a PV module (Fig. 2) being partially shaded. The simulation results are reported in in Fig. 8. As can be seen, when the irradiation of the shaded cell decreases from $G_{irr}$ =1000W/m$^2$ to $G_{irr}$ =267W/m$^2$, the current provided by the module drops from 7.5A to 2A. This value is maintained as long as the shading condition persists, that is during the time interval $\Delta T_s$, after which the correct current value is recovered. Instead, we can observe that $V_{mod}$ is kept to a constant value also while the shading condition occurs. Then, as soon as the shading is removed, the previous value of $I_{mod}$ is restored.

From the simulation results in Fig. 8, we can deduce that $V_{mod}$ is not suitable to be monitored in order to detect possible hot-spots, due to its negligible variation after the occurrence of a shading condition. Reversely, the current $I_{mod}$ is affected considerably as long as the shading condition persists. Therefore, as anticipated above, our proposed detection scheme is based on the idea to monitor the $I_{mod}$ current.

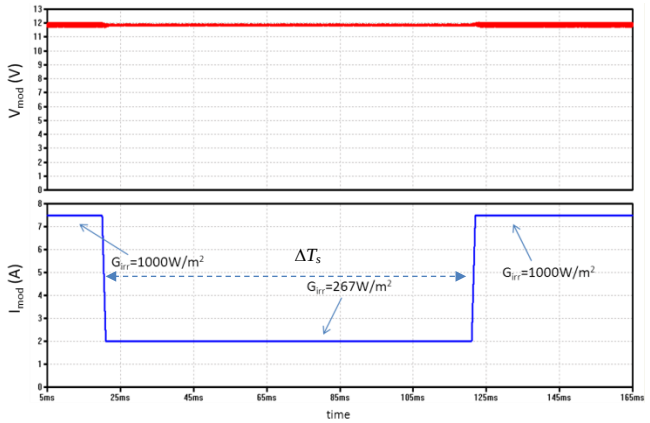


Fig. 8. Simulation results showing the behavior of the current $I_{mod}$ and the voltage $V_{mod}$ of the PV module in Fig. 2 when one of its PV cells becomes partially shaded.

### A. *Hot-Spot Detection Scheme Structure*

The structure of the proposed detection scheme is shown in Fig. 9. A current sensor $CS_i$ (i = 1..n) is connected to the output of each PV module $PVMOD_i$ (i=1..n). Each current sensor $CS_i$ gives as output a voltage Vi that is proportional to the current $I_{mod,i}$ sensed at the $PVMOD_i$ output. The voltage Vi is then compared, by means of an hysteresis comparator ($HCMP_i$), to a reference voltage ($V_{ref}$) provided by a reference current sensor $CS_{ref}$. The sensor $CS_{ref}$ measures the current ($I_{ref}$) produced by a reference cell. The measured current is equal to the current produced by the PV modules $PVMOD_i$ (i=1..n) under the same irradiation conditions. Of course, the reference cell should be properly selected, in order to be exempt from systematic shading, for instance due to the surrounding environment (e.g., antennas, trees, etc.), as well as from casual shading events (e.g., tree leaves, bird drops, etc.). The output of comparators $HCMP_i$ ($hs_i$) are then collected by a NOR gate, which generates an alarm signal NHS if at least one module undergoes a hot-spot condition.

The sensor must not alter the value of the power provided by the PV module to the respective MPPT block, in order not to affect the power efficiency of the whole PV system. Therefore, as discussed in the following subsection, the current sensors $CS_i$ have been implemented by means of Hall Effect sensors [25]. They sense the magnetic field induced by the current generated by the PV module, and produce an output voltage proportional to the sensed magnetic field.

More in details, the hysteresis comparators CMPi produce at their outputs $hs_i$:

$$hs_i = 0\ (0V),\ \text{if}\ I_{mod,i} \geq I_{ref}\ \ (V_i = kI_{mod,i} \geq V_{ref} = kI_{ref})$$
$$hs_i = 1\ (V_{cc}),\ \text{if}\ I_{mod,i} < I_{ref} - I_{th}\ (V_i = kI_{mod,i} < V_{ref} - V_{th} = k(I_{ref} - I_{th}), \quad (5)$$

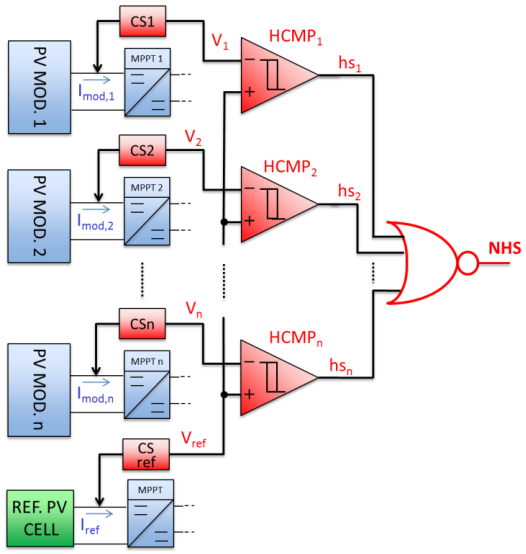


Fig. 9. Schematic representation of the proposed hot-spot detection scheme.

where, $I_{th}$ is a proper threshold current and k [V/A] is the equivalent transresistance of the Hall Effect current sensors. As shown later, the value of $I_{th}$ must be chosen by evaluating the minimum value of the radiation density $G_{irr}$ during a shading condition giving rise to a hot-spot.

This way, if all PV modules and the reference cell are equally irradiated, then all PV modules produce a current value equal to $I_{ref}$, and all comparators $HCMP_i$ give to their outputs $hs_i = 0$, $\forall i = 1..n$. Therefore, the detection scheme output NHS remains at its high logic value (NHS=1), denoting that no hot-spot condition has occurred.

Instead, if the i-th PV module undergoes a hot-spot condition, the provided current $I_{mod,i}$ turns out to be lower than $I_{ref}$. As a consequence, the output of the *i-th* comparator, $hs_i$, switches to 1, and the output of the detection scheme NHS goes to zero, thus generating a hot-spot alarm.

It is worth noticing that the signals $hs_i$ can also be employed for diagnosis purposes. In fact, they allow to identify the PV module undergoing a hot-spot condition. Therefore, when NHS = 0 (hot-spot alarm), a proper recovery mechanism can be activated (for instance based on bypassing the affected PV module), thus allowing to avoid the permanent damage of the cells under hot-spot, and therefore their impact on the power efficiency of the entire PV system.

It should be noted that, since the proposed hot-spot detection approach relies in the comparison between current/voltage of the PV module and a reference PV cell, its application is not limited by the considered MPPT method. Particularly, if the frequently used approach based on *perturb and observe* [26] is considered, we can reasonably expect that the difference between the values of current/voltage of the monitored PV module and the reference one is always smaller than the mismatch tolerated by the proposed hot-spot detection scheme (Fig. 9).

### *B. Proposed Scheme Implementation and Validation*

We have implemented and validated the proposed hot-spot detection scheme by means of SPICE simulations. The implemented PV modules to be monitored consist of 36 series cells (Fig. 2), modeled as described in Sect. 2. The same model has been used to implement the reference PV cell. We have implemented the MPPT connected to each monitored PV module and to the reference cell as described in Subsection 2.2 ( Fig. 3).

The hysteresis behavior of the $HCMP_i$ block described in (5) has been obtained as represented in Fig. 10. The voltage $V_{ref}$ generated by the reference circuit is diminished by a threshold $V_{th} = kI_{th}$ by means of a standard subtractor SUB. Then, the obtained value $V_{ref}' = V_{ref} - V_{th}$ is given to the input of a standard comparator $CMP_i$ of the kind in [27], together with the value $V_i$ coming from the current sensor of the $PVMOD_i$ ($i$ = 1..n) module.

As for the current sensors $CS_i$ ($i$ = 1..n) and $CS_{ref}$ in Fig. 9 they have been implemented by means of Hall effect current sensors of the kind in [25]. Each sensor measures indirectly the current produced by the PV array by measuring its associated magnetic field [25]. Then, as indicated in (5), the sensors give to their outputs a voltage $V_i = kI_{mod,i}$ ($i$=1..n), where $k$ is the equivalent transresistance of the Hall Effect current sensors. As power supply, we have used a voltage of 5V. All signals produced by the comparators ($hs_i$, i=1..n) feed a NOR gate generating an indication of hot-spot affecting a PV cell. This way, it is NHS = 1 (i.e., 5V), if none of the cells of a PV module is affected by a hot-spot condition, or NHS =0 (i.e., 0V), when one (or more) PV cells of a module is (are) under hot-spot.

We have performed electrical simulations to determine the threshold $V_{th} = kI_{th}$, where $k$=667mΩ, for which the irradiation density $G_{irr}$ of a shaded cell undergoing a hot-spot condition gives rise to a temperature increase up to 150°C. This irradiation value has been denoted by $G_{irr\text{-}150}$.
Particularly, within a PV module, the cell with a low shunt resistance undergoing a hot-spot condition is uniformly shaded, while the rest of the cells in the PV module are fully irradiated with $G_{irr}$ = 1000W/m$^2$. The obtained results are shown in Fig. 11. For $G_{irr}$ = 1000W/m$^2$, the operating temperature is 60°C. As the $G_{irr}$ of the low shunt resistance shaded cell (undergoing a hot-spot condition) decreases, the generated current decreases as well. As a consequence, the reverse voltage applied to the shaded cell turns out to increase (in absolute value). Therefore, also the power dissipated in the

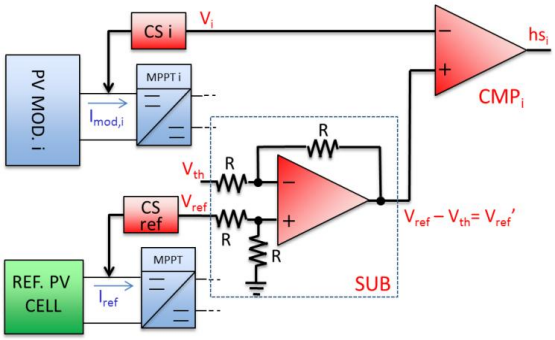


Fig. 10. Proposed implementation of the hysteresis comparators in HCMPi.

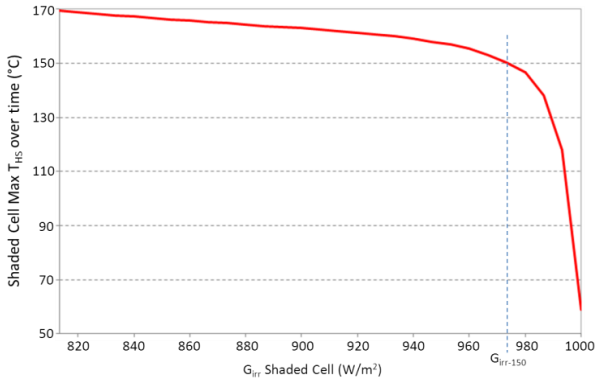


Fig. 11. Temperature increase in the cell area under hot-spot in a shaded cell, as a function of the cell irradiation density.

low shunt resistance area increases, rising up the temperature of the cell area undergoing a hot-spot condition. Particularly, the irradiation density $G_{irr-150}$ is equal to 972W/m$^2$. Afterwards, the threshold current $I_{th}$ has been obtained by introducing $G_{irr-150}$ in (1), and by simulating the circuit in Fig. 1(a). As a result, a value of $V_{th}$=200mV has been derived.

Fig. 12 reports some results of the simulation performed to validate the proposed hot-spot detection scheme. For simplicity, only the value of the reference cell and the PV module PV-MOD2 are shown. As an example, at the instant $t_1$, we have emulated the occurrence of a uniform shading of the whole PV system with a $G_{irr}$ = 746W/m$^2$, which can for instance occur in a cloudy day. As can be seen, the output currents of both the reference cell and the monitored PV modules decrease from 7.5A (the value corresponding to $G_{irr}$ = 1000W/m$^2$) to 5.6A. Meanwhile, the output voltages provided by the current sensors connected to PV-MOD2 ($V_2$) and $V_{ref}' = V_{ref} - V_{th}$ decrease, yet maintaining the voltage difference $V_{th}$ they presented before $t_1$. In this case, the comparator CMP2 keeps on producing $hs_2$ = 0, and the alarm signal NHS remains high, indicating a hot-spot free condition. The same considerations hold true between $t_2$ and $t_3$, where the maximum $G_{irr}$ is again reached.

Instead, after the instant $t_3$, a hot-spot condition affecting PV-MOD2 occurs, and the current generated by PV-MOD2 drops to a value considerably lower than that produced by the reference cell. Similarly, the output signal of the current sensor CS2 diminishes to a value lower than $V_{ref}'$. As a consequence, the output produced by the comparator CMP2 switches from 0 to 1, and the output NOR gate generates the alarm signal NHS = 0. The correct behavior of PV-MOD2 is recovered as soon as the shading conditions inducing a hot-spot are removed after the time instant $t_4$.

The detection of a hot-spot condition is the first step towards the possible activation of countermeasures to counteract this phenomenon. In this regard, in order to avoid permanent efficiency loss, after the detection of a hot-spot condition, the affected PV module could be by-passed by activating a proper switch [18, 19]. Then, after some time, a verification procedure could be activated in order to verify whether the hot-spot conditions still persist. If this is the case, a procedure for the manual removal of the hot-spot condition

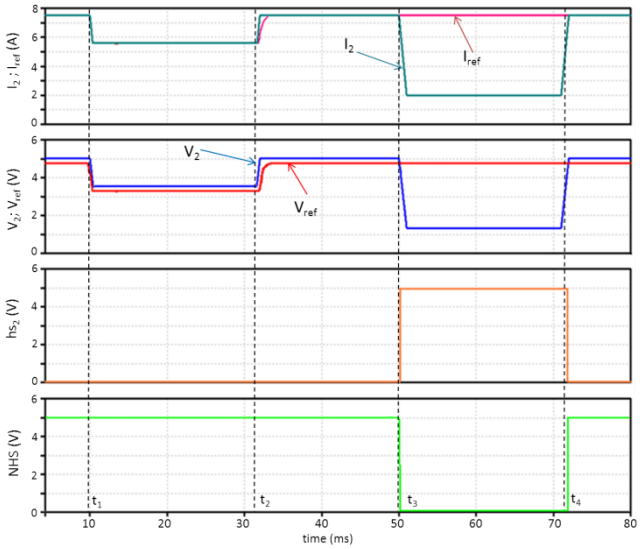


Fig. 12. Simulation results showing the behavior of the proposed hot-spot detection scheme in case of uniform shading ($t_1$-$t_2$), normal irradiation ($t_2$-$t_3$), and hot spot-condition ($t_3$-$t_4$)

could be actuated. The bypass of the PV module experiencing a hot-spot will introduce a temporary efficiency loss, but it will prevent the PV module from incurring a permanent damage, thus avoiding a permanent efficiency loss.

## VI. Conclusions

We first have addressed the problem of modeling the thermal behavior of PV cells that, due to their being exposed to shading, may experience a dramatic temperature increase (a phenomenon referred to as hot-spot) with consequent reduction of the provided power. Our model has been validated against experimental data. It has highlighted that, differently from what may be expected, a partially shaded PV cell enters the hot-spot condition faster than a fully shaded PV cell, thus providing useful hints that should be considered to design a highly energy efficient PV array.

We have then proposed a hot-spot detection scheme, which has been validated by means of electrical level simulations. Our scheme allows to detect the occurrence of a hot-spot affecting one of the PV module of the considered PV system, and to identify the affected module. This enables the possible activation of proper recovery mechanisms aimed at avoiding the damage of the module under hot-spot, as well as the drawback of the PV module under hot-spot on the power efficiency of the entire PV power generator system.

## References

[1] A. Kovach, J. Schmid, "Determination of energy output losses due to shading of building-integrated photovoltaic arrays using a raytracing technique," *Solar Energy*, vol. 57, no.2, pp. 117-124, 1996.

[2] M.C. Alonso Garcìa, W. Herrmann, W. Bohmer, "Thermal and Electrical Effects Caused by Outdoor Hot-spot Testing in Associations of Photovoltaic Cells," Progress in Photovoltaic: Research and Applications, 2003, pp. 293-307.

[3] H. Yang, W. Hu, H. Wang an M. Narayanan, "Investigation of reverse current for crystalline silicon solar cells. New concept for a test standard about the reverse current," 978-1-4244-5892-9/10/ 2010 IEEE.

[4] S. Silvestre, A. Chouder, "Shading Effects in Characteristic Parameters of PV Modules," in *Proc. of 2007 Spanish Conference on Electron Devices*, 2007, pp. 116-118.
[5] J. W. Bishop, "Computer simulation of the effects of electrical mismatch in photovoltaic cell interconnection circuits," *in Proc. of Solar Cell Conference*, 1988, pp. 73-79.
[6] S. Wendlandt, A. Drobisch, T. Buseth, S. Krauter and P. Grunow, "Hot spot risk analysis on silicon cell modules," in *Proc. of 25th European Photovoltaic Solar Energy Conference and Exhibition*, 2010, pp. 4002-4006.
[7] A. Simo and S. Martinuzzi, "Hot Spot and heavily dislocated regions in multicrystalline silicon cells," *PSC*, 1990, pp. 800-805.
[8] Y. Liu, B. Li, D. Zhong, "Research on Domestic PV Module Structure Based on Fault Detection," in *Proc. of 2010 8th World Congress on Intelligent Control and Automation (WCICA)*, 2010, 171-175.
[9] Y. Liu, B. Li, Z. Cheng, "Research on PV Module Structure Based on Fault Detection," in *Proc. of 2010 Chinese Control and Decision Conference (CCDC)*, 2010, pp. 3891-3895.
[10] D. Giaffreda, M. Omaña, D. Rossi, C. Metra, "Model for Thermal Behavior of Shaded PV Cells Under Hot-Spot Condition," in *Proc. of IEEE International Symposium on Defect and Fault Tolerance in VLSI and Nanotechnology Systems*, 2011, pp.252-258.
[11] Zhang Mei-xia, Yang Xiu "Efficiency Optimization of Photovoltaic Arrays Based on Distributed Max Power Point Tracking," in *Proc. of IEEE Innovative Smart Grid Technologies - Asia (ISGT Asia) Conference*, 2012, pp. 1-6.
[12] R. Ramaprabha, B.L. Mathur, "Development of an Improved Model of SPV Cell for Partially Shaded Solar Photovoltaic Arrays," *European Journal of Scientific Reserch*, ISSN 1450-216X Vol.47 No.1 (2010) pp. 122-134.
[13] J.A. Gow, C.D. Manning, "Development of a photovoltaic array model for use in power electronics simulation studies," *IEEE Proc.-Electr. Power Appl.* Vol. 146, No. 2, March 1999.
[14] P. Junsangsri and F. Lombardi, "Time/Temperature Degradation of Solar Cells under the Single Diode Model," in *Proc. of 25th International Symposium on DFT in VLSI Systems*, 2010, pp. 240-248.
[15] P. Junsangsri and F. Lombardi, "Double Diode Modeling of Time/Temperature Induced Degradation of Solar Cells," in *Proc. of* 53rd IEEE International MWSCAS, 2010, pp.1005-1008.
[16] M. Danner, K. Bucher, "Reverse characteristics of commercial silicon solar cells – Impact on hot spot temperature and module integrity," Photovoltaic Specialists Conference, 1997, pp. 1137-1140.
[17] T. Shimizu, M. Kamezawa, H. Watanabe, "Generation Control Circuit for Photovoltaic Modules," *IEEE Transactions on Power Electronics*, vol. 16, NO. 3, May 2001.
[18] R. Candela, V. Di Dio, E. Riva Sanseverino, P. Romano, "Reconfiguration Techniques of Partial Shaded PV Systems for the Maximization of Electrical Energy Production," in *Proc. of IEEE International Conference on Clean Electrical Power*, 2007, pp. 716-719.
[19] A. Bidram, A. Davoudi, R. S. Balog, "Control and Circuit Techniques to mitigate Partial Shading Effects in Photovoltaic Arrays," *IEEE Journal of Photovoltaics*, vol. 2, no. 4, Oct. 2012, pp. 532-546.
[20] J. Wohlgemuth and W. Herrmann, "Hot spot test for crystalline silicon modules," *PSC 2005*, pp. 1062-1063.
[21] S. Armstrong, W.G. Hurley, "A thermal model for photovoltaic panels under varying atmospheric conditions," *Applied Thermal Engineering* (2010), pp. 1488-1495.
[22] W. Knaupp, "Evaluation of PV Module Designs at Irregular Operation Conditions", in *Proc. of IEEE Photovoltaic Specialists Conf.*, pp. 1213-1216, 1997.
[23] J. Hudson, L. Vasilyev, J. Smidt, G. Horner, "Economic Impacts and Approaches to Address Hot-Spot Defects in Photovoltaic Devices", in *Proc. of IEEE Photovoltaic Specialists Conf.*, pp. 1706 – 1709, 2010.
[24] D. Giaffreda, P. Magnone, M. Meneghini, M. Barbato, G. Meneghesso, E. Zanoni, E. Sangiorgi, C. Fiegna, "Local Shunting in Multicrystalline Silicon Solar Cell: Distributed Electrical Simulatoins and Experiments," *IEEE Jour. of Photovoltaics*, vol. 4, no. 1, Jan. 2014, pp. 40-47.
[25] C. Xiao, L. Zhao, T. Asada, W. G. Odendaal, J. D. van Wyk, "An Overview of Integratable Current Sensor Technologies," Conference Record of the Industry Applications Conference, 2003, vol. 2, pp. 1251-1258.
[26] K.H., Hussein, I. Muta, T. Hoshino, M. Osakada, "Maximum photovoltaic power tracking: an algorithm for rapidly changing atmospheric conditions,", IEE Proceedings- Generation, Transmission and Distribution, vol. 142 , no. 1, 1995, pp. 59-64.
[27] T. Yu Lo, C. Chih Hung, "1.5-V Linear CMOS OTA with-60dB IM3 for High Frequency Applications," in Proc. of IEEE Solid State Circuits Conference, 2006, pp. 167-170.

**Daniele Rossi** received the degree in electronic engineering and the PhD degree in electronic engineering and computer science from the University of Bologna in 2001 and 2005, respectively. He is currently a Post-Doctoral fellow at the same University. His research interests include fault modeling and fault tolerance, focusing on coding techniques for fault-tolerance and low-power, signal integrity for communication infrastructures, robust design for soft error resiliency.

**Martin Omaña** received the degree in electronic engineering from the University of Buenos Aires in 2000. In 2002 he was awarded a MADESS grant and joined the University of Bologna, where he obtained the PhD in Electronic Engineering and Computer Science in 2005. He is currently a Post-Doctoral fellow at the same University. His research interests are in the field of fault modeling, on-line test, robust design, fault tolerance and photovoltaic systems.

**Daniele Giaffreda** received the M.S. degree in electronic engineering from the University of Bologna, Italy in 2009. He is currently working as Ph.D. student at the Advanced Research Center on Electronic Systems for Information and Communication Technologies (ARCES) E. De Castro, University of Bologna, Bologna, Italy. His research interests include faults modelling and electrical simulations with particular emphasis on the silicon photovoltaic solar cell.

**Cecilia Metra** (F'14) is a Professor of Electronics with the University of Bologna, Bologna, Italy. Her current research interests include fault modeling, on-line test, robust design, fault tolerance, energy harvesting, and photovoltaic systems.
Prof. Metra is a Vice-President for Technical and Conference Activities of the IEEE Computer Society (CS) for 2014, and a member of the Board of Governors of the IEEE CS 2013-2015. Since 2013, she has been Editor-in-Chief of the IEEE CS online publication Computing. She is a Golden Core Member of the IEEE CS.